Contribution to the AMS-10, Berkeley for Poster P. Steier et al., "AMS of $^{41}$Ca and $^{36}$Cl at a 3-MV tandem with a ΔTOF detector" in Poster Session 2

# AMS of $^{36}$Cl at a 3-MV tandem with a ΔTOF detector

Peter Steier[1,*], Robin Golser[1], Walter Kutschera[1], Tobias Orlowski[1], Alfred Priller[1], Lena Siebert[1], Christof Vockenhuber[2], Anton Wallner[1]

[1] Vienna Environmental Research Accelerator (VERA), Institut für Isotopenforschung und Kernphysik der Universität Wien, Währinger Straße 17, A-1090 Wien, Austria

[2] TRIUMF Laboratory, 4004 Wesbrook Mall, Vancouver, BC, V6T 2A3, Canada

## Abstract

For the first time, we demonstrated the possibility to detect $^{36}$Cl at natural isotopic concentrations at a 3-MV tandem AMS system. With the method of ΔTOF, the residual energy of initially mono-energetic ions is measured precisely with a time-of-flight detector after passing through an absorber foil. Differences in the specific energy loss lead to a clear separation of $^{36}$Cl from the isobar $^{36}$S though we cope with energies below 1 MeV/amu. Systematic studies helped to optimize the ΔTOF setup. The use of silicon nitride foils results in residual energy spectra which are almost free of tails. A suppression of $^{36}$S of 500 was achieved at a detector efficiency of 9%. With an improved chemical sulfur suppression we obtained a ratio of $^{36}S^-/^{35}Cl^- = 5\times10^{-11}$. In a first test measurement, the sulfur-induced background for $^{36}$Cl/Cl was in the order of $10^{-13}$. The sensitivity limit was imposed by a $^{36}$Cl cross contamination of ~1% from the standard to the blank.

Keywords: $^{36}$Cl, AMS, ΔTOF, isobar separation

PACS: 29.30.Aj; 29.17.+w

* Corresponding Author:

Peter Steier

Vienna Environmental Research Accelerator (VERA), Insitut für Isotopenforschung und Kernphysik der Universität Wien, Währinger Straße 17, A-1090 Wien, Austria

Tel.: +(43)-1-4277-51729

Fax: +(43)-1-4277-9517

e-mail: peter.steier@univie.ac.at

## Introduction

Continuing technical progress has allowed medium size (~3 MeV) accelerators to measure all AMS isotopes where no stable isobar forming negative ions exists [1]. Sensitivity and precision are competitive to larger facilities. However, suppression of a stable isobar at the detector was only possible for the lightest AMS ion $^{10}$Be (with $^{10}$B the stable isobar). This limitation is caused by the process usually applied for separation, i.e. the different energy loss in matter. For energies below the maximum of the Bragg curve (~1 MeV/amu) the energy straggling was thought to exceed the separation. However, recent investigations [2] show that in many cases this expectation is not true.

ΔTOF is a new method for isobar separation at energies below 1 MeV/amu [3]. The residual energy of initially mono-energetic ions is measured precisely with a time-of-flight detector. ΔTOF is superior to other methods, since angular straggling and charge state variations do not reduce the measurement precision. Additionally, the energy resolution can be made arbitrarily high by increasing the flight path. This allows studying the physical limitations due to energy straggling independently from detector properties, though at reduced efficiency. Since the goal of the present work was to develop competitive $^{36}$Cl measurements, a compromise between separation and efficiency was sought. Systematic studies have led to an optimized ΔTOF setup.

$^{36}$Cl is probably the best test case for the potential of the ΔTOF method. The stable isobar $^{36}$S has to be suppressed by chemistry and in the detector, since sulfur forms abundant negative ions. For another AMS isotope, $^{41}$Ca, a first successful application of the ΔTOF method is presented in a separate paper to this proceedings [4].

## The ΔTOF setup

Figure 1 show a schematic of the ΔTOF setup. Different from [3], the energy absorber is now placed after the start detector. This avoids a "dead" flight path after the absorber which is not used for the energy measurement, but where the straggled ions diverge already. The remaining flight path is 0.63 m, and the stop detector was rotated so that the ions pass through the grids of the electron mirror before reaching the foil. By these means, we can not only detect ions which pass through the mesh supported DLC foil [5] of 18 mm diameter, but also ions which hit the mesh (10% of the area) or even the surrounding foil holder. By moving the detector up and down, an active diameter of 25 mm was observed, which agrees with the nominal active area of the multi-channel plates (MCPs) used. By these means, ions up to a scattering angle of 20 mrad can be detected. In this setup, the stop detector detects electrons which are emitted backwards.

The ionization chamber placed after the stop detector has an entrance window of 10 mm diameter and accepts only a small part of ions entering the start detector. Thus, the detection efficiency is much lower if coincident signals from both detectors are required. Additionally, the relatively low energy resolution of the chamber used (~1 μm Mylar window with aluminum coating) does not provide any additional separation between $^{36}$Cl and $^{36}$S. Thus, the chamber serves only as an indicator whether any interference with the same velocity, but at lower energy (e.g. from mass/charge ambiguities) is present. Fortunately, in the case of $^{36}$Cl$^{7+}$ no such ions were detected.

The stop detector is equipped with a thin DLC foil (2 μg/cm$^2$). For the start detector, systematic investigations were performed to find the best suited foil, because low-energy tails

were observed in previous experiments. We attributed at least a part of the observed tails to the supporting mesh of the start foil.

Silicon nitride membranes (Silson Ltd, Northampton, UK) with the likely composition $Si_{3.0}N_{3.1}H_{0.06}$ [6] used both in the start timing detector and as energy absorbers have proven to be extremely homogenous. The peaks in the residual energy spectra (see Figure 2) are almost free of tails. With a 1000 nm thick silicon nitride membrane mounted directly into the start detector and used as secondary electron emitter also, a TOF peak of perfectly Gaussian shape is obtained. We attribute this to the smoothness of the surfaces and to the amorphous structure, which avoids grain boundaries and channeling.

However, in this setup, a large fraction of the ions (20% to 90%) passes the membrane without producing detectable secondary electrons, despite several 100 electrons per ion are expected [7]. We attribute this to the insulating properties of the silicon nitride. The membrane charges up locally to several kV, which prevents low-energy electrons to escape. Assuming a perfect insulator, the average number of electrons emitted has to balance the number of electrons lost in the ion stripping process in the membrane. Thus, only very few electrons per ion can be expected in the cases we have investigated.

To avoid an insulating timing foil, we have tried two options which both provided ~100 % detection efficiency for transmitted ions (see Figure 2):

1) Use of carbon foils. Despite the carbon foil (15 μg/cm$^2$) was much thinner than the SiN foils used as energy absorber, a long low energy tail is produced.

2) Deposition of a conducting material onto a silicon nitride membrane. A coating with light atoms is preferable with respect to straggling and scattering. However, a first attempt with a vacuum deposited carbon layer failed. Electron microscope images revealed a scaly structure probably due to bad adhesion to the substrate. Thus we took resort to an aluminum layer, which was deposited by the manufacturer of the silicon nitrate membrane. The aluminum (estimated thickness 20 nm) still introduces some low energy tails, but gives acceptable results. For the $^{36}$Cl measurements presented in this paper, the start detector was equipped with a 50 nm silicon nitride foil coated with approximately 25 nm Al.

The energy absorber consists of three foil stacks which can be inserted independently. By equipping the foil stacks with silicon nitride foils of nominally 750 nm (500 nm+150 nm+100 nm), 1500 nm (1000 nm+500 nm), and 3000 nm (3×1000 nm), respectively, seven different absorber thicknesses can be selected without breaking the vacuum. In practice, the energy losses calculated by SRIM [8] do not agree with the measurements (see Figure 3). All foils showed less energy loss than calculated. We cannot decide whether our calculations overestimate the energy loss or whether the membranes are effectively thicker than nominally. However, we can compare the relative energy loss of the foils. It turns out that the three foil stacks do not show thickness ratios of 1:2:4, but rather 1.087:2.000:3.987. Thus, for self-consistency of this paper, we use the values 815 nm, 1500 nm, and 2990, respectively (1500 nm was chosen arbitrarily as the reference).

Figure 4 shows the separation achieved for $^{36}$Cl and $^{36}$S at an initial energy of 28 MeV. Due to increasing scattering, the detector efficiency decreases from ~60 % without energy absorber to ~6 % with 4540 nm silicon nitride. For the $^{36}$Cl measurement presented in the following we chose 3855 nm (incl. 50 nm start timing foil), which resulted in a detector efficiency of 9 %. The separation of $^{36}$Cl and $^{36}$S is close to 2 FWHM.

## Sample preparation

Since the experiments described in [1] we have developed a procedure for the preparation of chlorine sputter targets which are low in sulfur. The AgCl sputter target (~2 mm diameter) is surrounded by a AgBr surface of 7 mm diameter (Figure 5b), which guards against sulfur sputtering from the sample holder and wheel. Both the AgBr and the AgCl (produced from NaCl, and NaBr, respectively) are purified with the same chemical procedure to suppress sulfur. Figure 6 gives the flow chart.

Prior to use, all tools and beakers used are stored in detergent over night and rinsed with $H_2O$ bidest. The sample solution as well as all reagents used ($AgNO_3$, NaCl, and NaBr) are prepared as solutions in 2 M $HNO_3$ + 0.1 M $Ba(NO_3)_2$. By adding $Ba(NO_3)_2$ to all ingredients, followed by storage and filtration, sulfur is precipitated and removed as $BaSO_4$ ($S^+$ and $SO_x^-$ are oxidized to $SO_4^{2-}$ by the $HNO_3$). A small piece of quartz filter is added during storage to increase the surface for attachment of precipitated $BaSO_4$. The $Cl^-$ (or $Br^-$) solution and the $Ag^+$ solution are filtered through separate quartz filters with $N_2$ overpressure directly into the same centrifuge tube, where precipitation of AgCl (or AgBr, respectively) takes place. As funnels for this filtration, we used pipette pins plugged with small pieces of quartz filters. Also for washing of the precipitate, a similarly filtrated $Ba(NO_3)_2$ solution is used instead of water. Thus, a certain amount of $Ba(NO_3)_2$ remains in the sputter targets, which, however, did not cause any problems in the AMS measurement. The AgBr and the AgCl are dried over night at 60 °C.

A bed of AgBr covering an area of 7 mm diameter is pressed into a stainless steel holder (see Figure 5). The AgCl sample is pressed into a small dimple (1 mm diameter) in the center. The plasticity of AgBr and AgCl leads to an effective sample diameter of 2 mm. Up to now, only very few sputter targets were prepared with this procedure. No systematic investigations on the influence of the various parameters of the procedure (e.g. storing time, filtration speeds, filter type) were performed yet.

In a test measurement for the chemical procedure, sputter targets were produced from AgCl with 7 mm diameter. The $^{36}S$ contamination was measured at VERA with a simplified setup. Instead of ΔTOF, a silicon surface barrier detector was used and the $^{36}S^{5+}$ count rate was measured. 100 % detector efficiency can be assumed for this detector. A $^{36}S^{5+}/^{35}Cl^{5+}$ ratio of $2.5\times10^{-13}$ was observed. Unfortunately, a similar chemical sulfur suppression was not achieved for the AgCl/AgBr targets, which we investigated with the ΔTOF system. For those, a $^{36}S^{7+}/^{35}Cl^{7+}$ of $\sim5\times10^{-11}$ was observed.

## AMS measurement

In our MCSNICS ion source (NEC, Wisconsin) we have recently implemented the possibility to move the sputter target relatively to the cesium beam in fine steps [9]. This allows to scan over the sample surface and to study the spatial distribution of the sputtered ions. Figure 5a shows a scan over the cross section of our AgCl/AgBr targets. The AgBr shows a much lower sulfur content if compared to the copper of the wheel and especially to the stainless steel of the sample holder. In the future, we will manufacture sample holders from aluminum.

After initial problems with runaway conditions of the source (> 100 μA $^{35}Cl^-$) and sample melting we followed procedures developed at the ANU (Canberra, Australia) to operate the MC-SNICS ion source for Cl [10]. Rather low cesium energies (3 keV) must be used, but at normal cesium feeding levels. Control of the source output is possible with the ionizer power. By these means, we increased the source output slowly from ~1 to 20 μA $^{35}Cl^-$ during the measurement. Future measurements will be performed at ~10 μA.

Since higher charge states are populated at higher terminal voltages, the achievable energy grows faster than linear with the terminal voltage. The achievable energies can be approximated in the form $E \sim U^{1.3}$ [1]. Since high particle energy is crucial for isobar separation by energy loss, we are venturing for the maximum terminal voltage possible. Although VERA is nominally a 3-MV tandem, we can now work at 3.5 MV routinely. This voltage was also selected for the present measurement.

Stripper foils populate higher charge states than gas. This allows an additional gain in energy, and 28 MeV were obtained for $^{36}Cl^{7+}$ in the present measurement. It turned out that $^{36}Cl$ does not reach charge state equilibrium for our extremely thin DLC foils of only 0.5 μg/cm$^2$, and the 7+ yield was only ~10%. Better results were obtained with thicker C foils (2.6 μg/cm$^2$), produced by laser-plasma ablation [11]. The yield of 19% for $^{35}Cl^{7+}$ compares favorable to the 17% expected using the formula from [12]. After the tandem, the 7+ charge state has an energy of 28 MeV, which is already close to the Bragg maximum for $^{36}Cl$.

Fast sequential injection was used to measure $^{35}Cl^-$ in the injector and $^{35}Cl^{7+}$ and $^{37}Cl^{7+}$ in the analyzer offset Faraday cups. A technical detail worth to note is that we leave the injector offset cup at the position used for $^{13}C^-$ in $^{14}C$ measurements, and use the magnet chamber bias voltage to deflect $^{35}Cl^-$ to this position for a short time interval. By these means, we artificially increase the comparable small distance of the chlorine isotopes, and we can be sure that the offset cup does not interfere with $^{36}Cl^-$ when it is injected into the tandem.

$^{36}Cl^{7+}$ is measured in the ΔTOF detector which is installed in the heavy ion beam line of VERA [13]. However, the flight path set up for heavy isotope separation (3.64 m) is too long for ΔTOF of $^{36}Cl$. Thus, we have installed now a dedicated ΔTOF start detector and the absorber foil stack at a distances of 0.63 m before the common stop detector. Since all detectors are retractable, it is possible to switch between ΔTOF and heavy ions without venting the beam line.

Figure 7 shows the raw data with and without the residual energy signal from the ionization chamber. The results presented here are based solely on the TOF detector, since no background was observed in the ionization chamber.

The $^{36}Cl$ and the $^{36}S$ peaks are separated by 2.0 FWHM, which agrees with the systematic measurements presented above. A suppression factor of ~500 for $^{36}S^{7+}$ is achieved in the detector, at a detector efficiency of 9 % for $^{36}Cl^{7+}$.

Cross-talk from the standard was the limiting background in the present measurement. By fitting Gaussian distributions with exponential tails to the main peaks and by unfolding the blank spectrum, the cross contamination was quantified as ~1% from the standard to the blank (in the systematic measurements before, where the sputter times were significantly longer, values of several percent were observed). Additional evidence that the "shoulder" in the blank spectrum in Figure 7 is really caused by $^{36}Cl$ is given by the time variation of the content of the $^{36}Cl^{7+}$ integration bin compared to the $^{36}S^{7+}$ bin. If the shoulder was a structure of the detector response for $^{36}S$, the two bins should correlate. No such correlation is visible in the data.

We cannot yet say whether this is a memory-effect (i.e. the $^{36}Cl$ would decrease again if the measurement is paused on a Cl-free sputter target) or if this a real cross contamination (i.e. deposition of $^{36}Cl$ on the blank targets from the standard). As a first aid, in the further investigations lower standards will be used. However, we note that cross contamination of volatile chemical species like Cl (or I) is a problem inherent to the construction of the multi-cathode SNICS. The fact that all samples are mounted in the same sample wheel is an invaluable advantage as far as reliability and ease-of-use are concerned, but it implies that the samples are exposed to vapors released by the others.

## Summary and outlook

The measurement parameters for $^{36}$Cl achieved with ΔTOF at VERA are summarized in Table 1. The background for $^{36}$Cl/$^{35}$Cl caused by $^{36}$S is below $10^{-13}$. Since the contribution of this background can be precisely calculated from the count rate and shape of the $^{36}$S peak, we think that the present detection limit is almost $10^{-14}$. However, this must be bolstered by additional systematic measurements. Improvements of the $^{36}$S/$^{36}$Cl separation can still be expected, by further optimizing the ΔTOF geometry, the ion energy, and the absorber thickness. The regular AgBr-backed sputter targets used for the ΔTOF measurement showed a much larger sulfur contamination than large AgCl targets. This suggests that improvements can also be expected in the sample chemistry.

Despite these shortcomings, the present results demonstrate that in the case of $^{36}$Cl, 3-MV tandems will be able to perform competitive measurements for environmental samples.

Now that ΔTOF has proven the possibility of the separation, it might be advantageous to switch back to "conventional" detectors (e.g. state-of-the art ionization chambers, [14]) for the measurement of the residual energy after the silicon nitride absorber. Such a setup would hopefully combine the advantages of the silicon nitride membranes with the 100% efficiency of the ionization chamber.

## Acknowledgement

We thank Keith Fifield (ANU, Canberra, Australia), and Lukas Wacker and Martin Suter (PSI, Zürich, Switzerland) for fruitful discussion. The $^{36}$Cl standard solution was provided by the GAMS group at the TU Munich, Germany.

## References

[1] P. Steier, R. Golser, V. Liechtenstein, W. Kutschera, A. Priller, C. Vockenhuber, A. Wallner, Nucl. Instr. and Meth. in Phys. Res. B 240 (2005), 445.

[2] M. Suter, M. Döbeli, M. Grajcar, M. Stocker, H.-A. Synal, L. Wacker. Advances in particle identification in AMS at low energies. Contribution to these proceedings.

[3] C. Vockenhuber, R. Golser, W. Kutschera, A. Priller, P. Steier, K. Vorderwinkler, A. Wallner, Nucl. Instr. and Meth. in Phys. Res. B 240 (2005) 490.

[4] A. Wallner, I. Dillmann, R. Golser, F. Kaeppeler, W. Kutschera, M. Paul, A. Priller, P. Steier, C. Vockenhuber. Experimental Nuclear Astrophysics with AMS. Contribution to these proceedings.

[5] V.Kh. Liechtenstein, T.M. Ivkova, E.D. Olshanski, R. Golser, W. Kutschera, P. Steier, C. Vockenhuber, R. Repnow, R. von Hahn, M. Friedrich, U. Kreissig, Nucl. Instr. and Meth. in Phys. Res. A 521 (2004) 197.

[6] M. Doebeli, C. Kottler, M. Stocker, S. Weinmann, H.-A. Synal, M. Grajcar, M. Suter, Nucl. Instr. and Meth. in Phys. Res. B 219-220 (2004) 415.

[7] H. Rothard, K. Kroneberger, A. Clouvas, E. Veje, P. Lorenzen, N. Keller, J. Kemmler, W. Meckbach, K.–O. Groeneveld, Phys. Rev A 41 (1990) 2521.

[8] J.F. Ziegler, James Ziegler - SRIM & TRIM, http://www.srim.org/, accessed at 15.12.2005.

[9] A. Priller, M. Auer, R. Golser, A. Herschmann, W. Kutschera, J. Lukas, P. Steier, A. Wallner. Ion source refinement at VERA. Contribution to these proceedings.

[10] K. Fifield. 2005. Personal communication.

[11] P. Maier-Komor, A. Bergmaier, G. Dollinger, C.M. Frey, H.-J. Körner, Nucl. Instr. and Meth. in Phys, Res. A 397 (1997) 131.

[12] R. O. Sayer, Rev. de Phys. App. 12 (1977) 1543.

[13] C. Vockenhuber, I. Ahmad, R. Golser, W. Kutschera, V. Liechtenstein, A. Priller, P. Steier, S. Winkler. Int. J. Mass Spectrometry 223–224 (2003) 713.

[14] M. Stocker, M. Döebeli, M. Grajcar, M. Suter, H.-A. Synal, L. Wacker. Nucl. Instr. and Meth. in Phys. Res. B 240 (2005) 483.

## *Tables*

Table 1 Conditions for $^{36}Cl$ measurements at VERA

| | |
|---|---|
| Injected ion | $^{36}Cl^-$, $^{35}Cl^-$ (~10 μA) |
| Accelerator terminal voltage | 3.5 MV |
| Stripping | C foil, 2 μg/cm$^2$ |
| Analyzed ion | $^{36}Cl^{7+}$ (28 MeV) |
| Charge state yield (incl. transmission) | 19 % |
| ΔTOF absorber | 3855 nm SiN with Al coating |
| TOF path | 0.63 m |
| detector efficiency[1] | 9 % |
| Separation of $^{36}Cl^{7+}$ from $^{36}S^{7+}$ | 2.0 FWHM |
| Suppression factor of $^{36}S^{7+}$ | ~500 |
| Chemical suppression | $^{36}S^-/^{35}Cl^-$: ~$5\times10^{-11}$ |
| $^{36}S^{7+}$ induced background in $^{36}Cl^{7+}$ bin | ~$1\times10^{-13}$ for $^{36}Cl/^{35}Cl$ |

[1] defined as number of valid detector events inside $^{36}Cl^{7+}$ region-of-interest divided by number of $^{36}Cl^{7+}$ reaching the detector.

## *Figure captions*

Figure 1 Schematic of the ΔTOF detector system consisting of two MCP detectors and an ionization chamber. $E_0$, $v_0$, and $E_r$, $v_r$ indicate the energy and velocity before and after the absorber, respectively..

Figure 2 TOF spectra for different silicon nitride timing foils used in the start MCP detector. Solid curve: 1000 nm silicon nitride; dashed curve: 1000 nm silicon nitride plus 15 μg/cm$^2$ carbon foil; dotted curve: 1000 nm silicon nitride coated with aluminum (estimated thickness 20 nm).

Figure 3 Highest probability energy loss of Cl and S in silicon nitride. The data was obtained with $^{36}$S (■), $^{36}$Cl (O), and $^{37}$Cl (□). The $^{37}$Cl data is plotted at the energy of mass 36 with the same velocity. The solid and the dotted line are SRIM [8] calculations for transmitted $^{36}$Cl and $^{36}$S, respectively. The wiggles are an artifact of the Monte-Carlo calculation.

Figure 4 Measured separation (●) and FWHM (O) for $^{36}$S and $^{36}$Cl at 28 MeV initial energy after different thicknesses of silicon nitride.

Figure 5 Geometry of the sputter targets (b). (a) shows a position scan of the $^{36}S^{5+}$ count rate (solid line, left scale, logarithmic), together with the $^{35}Cl^-$ current (dashed line, right scale, linear). The horizontal axes of the plot is matched to the schematic. (1) AgCl sample, (2) AgBr backing, (3) stainless steel holder, (4) copper sample wheel, (5,6) neighboring holders.

Figure 6 Chemical purification scheme. Both the AgCl sample and the AgBr for the backing are produced by this procedure. All solutions are in 2M $HNO_3$.

Figure 7 Histograms of TOF vs. ionization chamber (a) and TOF only (b). In (a), the a measurement with a blank (black) and a standard ($^{36}$Cl/Cl = $10^{-10}$, gray) is overlayed. In (b), the spectra of a standard (solid line) and a blank (dashed line) were normalized for same $^{36}$S content. Gaussian distributions with exponential tails were fitted to the peaks (thin curves). Unfolding of the blank spectrum reveals cross contamination by $^{36}$Cl from the standard.

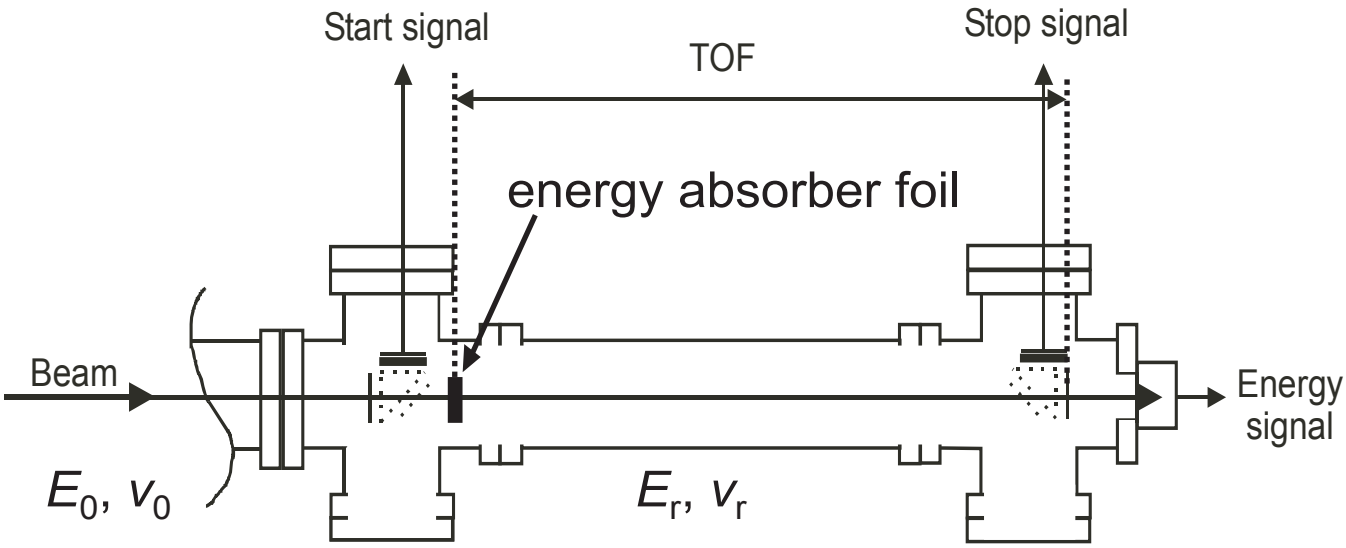
Start signal
TOF
Stop signal
energy absorber foil
Beam
Energy signal
$E_0$, $v_0$
$E_r$, $v_r$

Figure 1

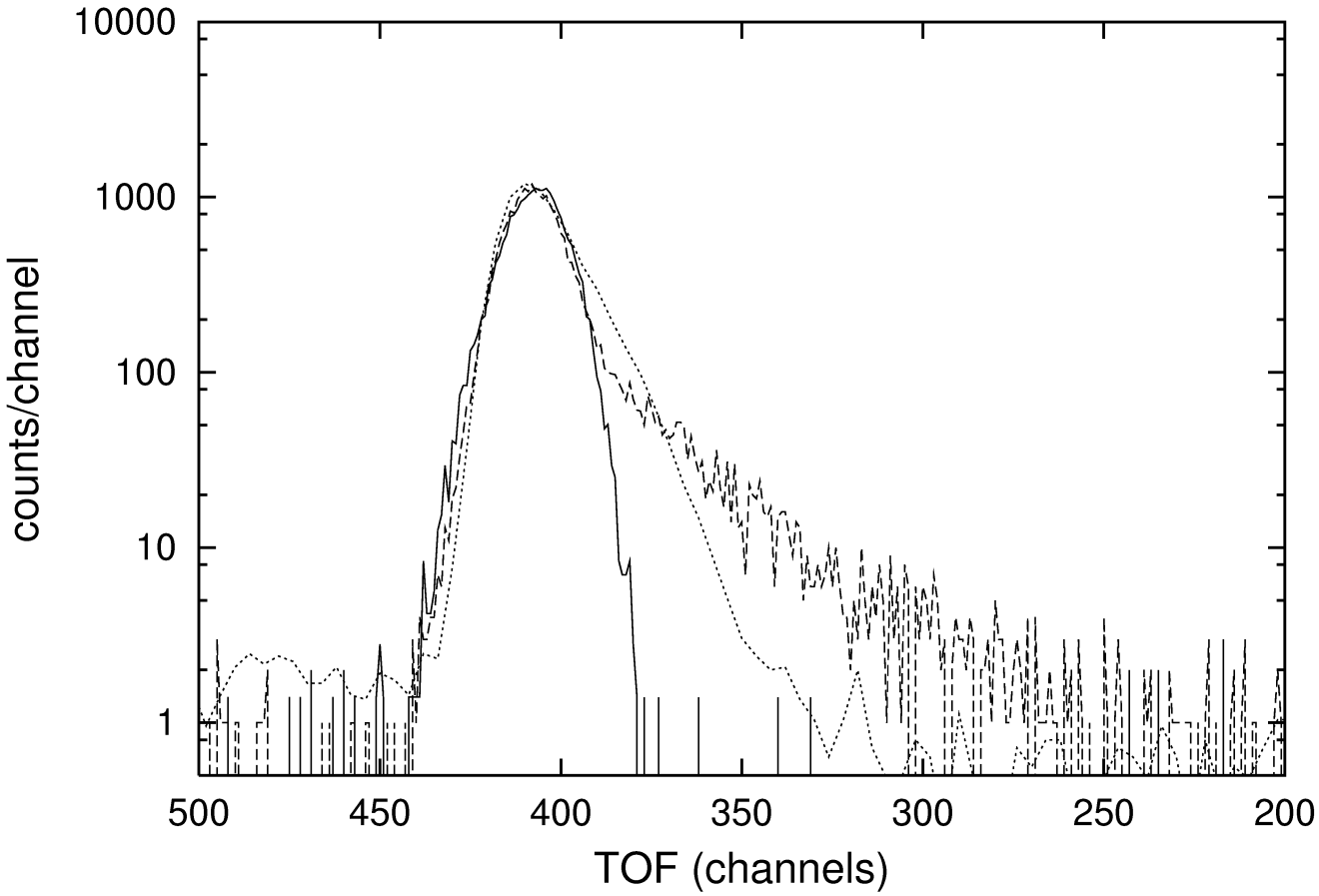
10000
1000
100
10
1
counts/channel
500
450
400
350
300
250
200
TOF (channels)

Figure 2

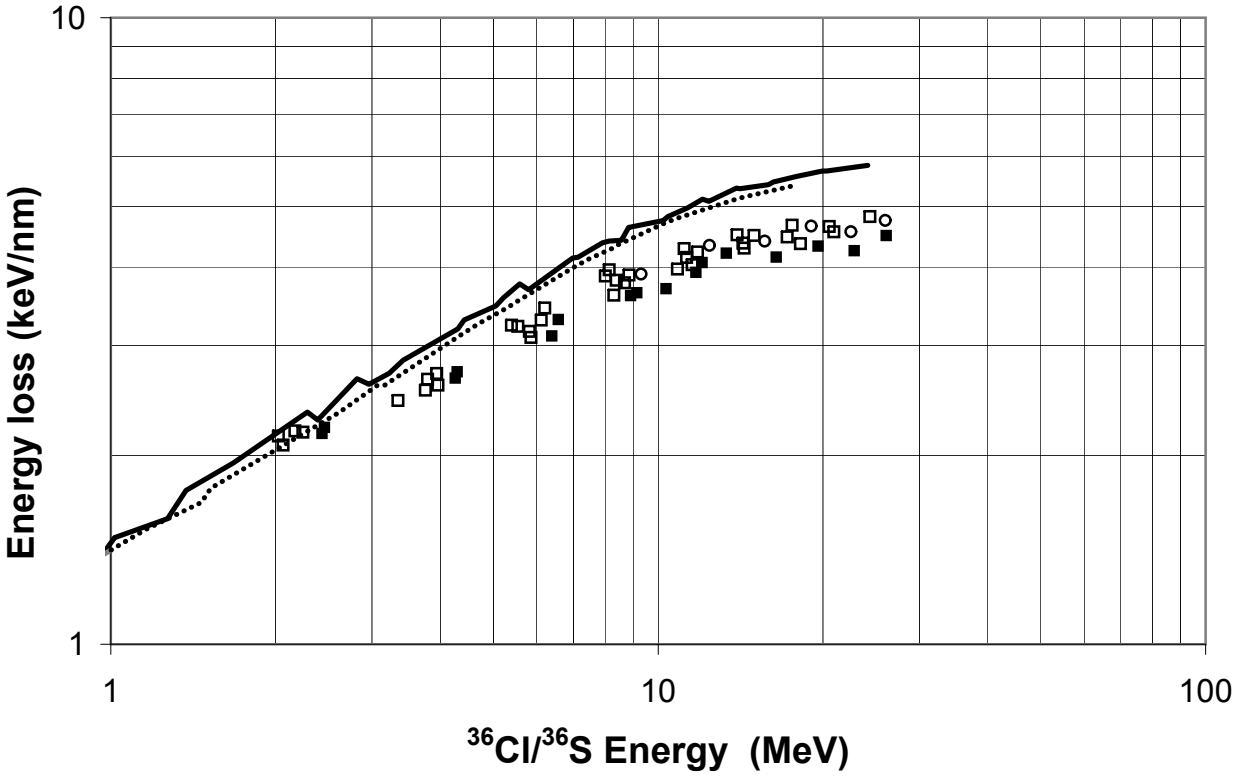


Figure 3

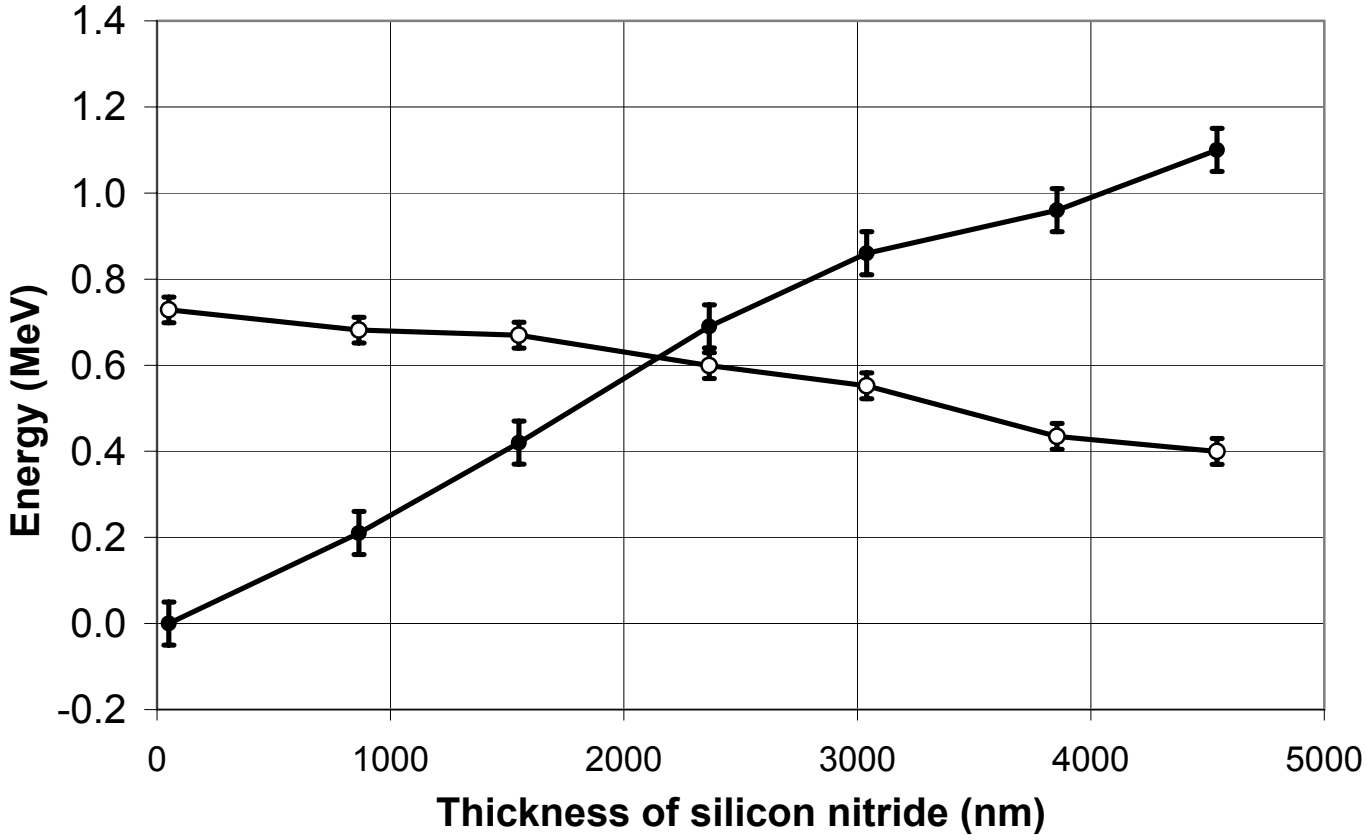
1.4
1.2
1.0
0.8
0.6
0.4
0.2
0.0
-0.2
Energy (MeV)
0
1000
2000
3000
4000
5000
Thickness of silicon nitride (nm)

Figure 4

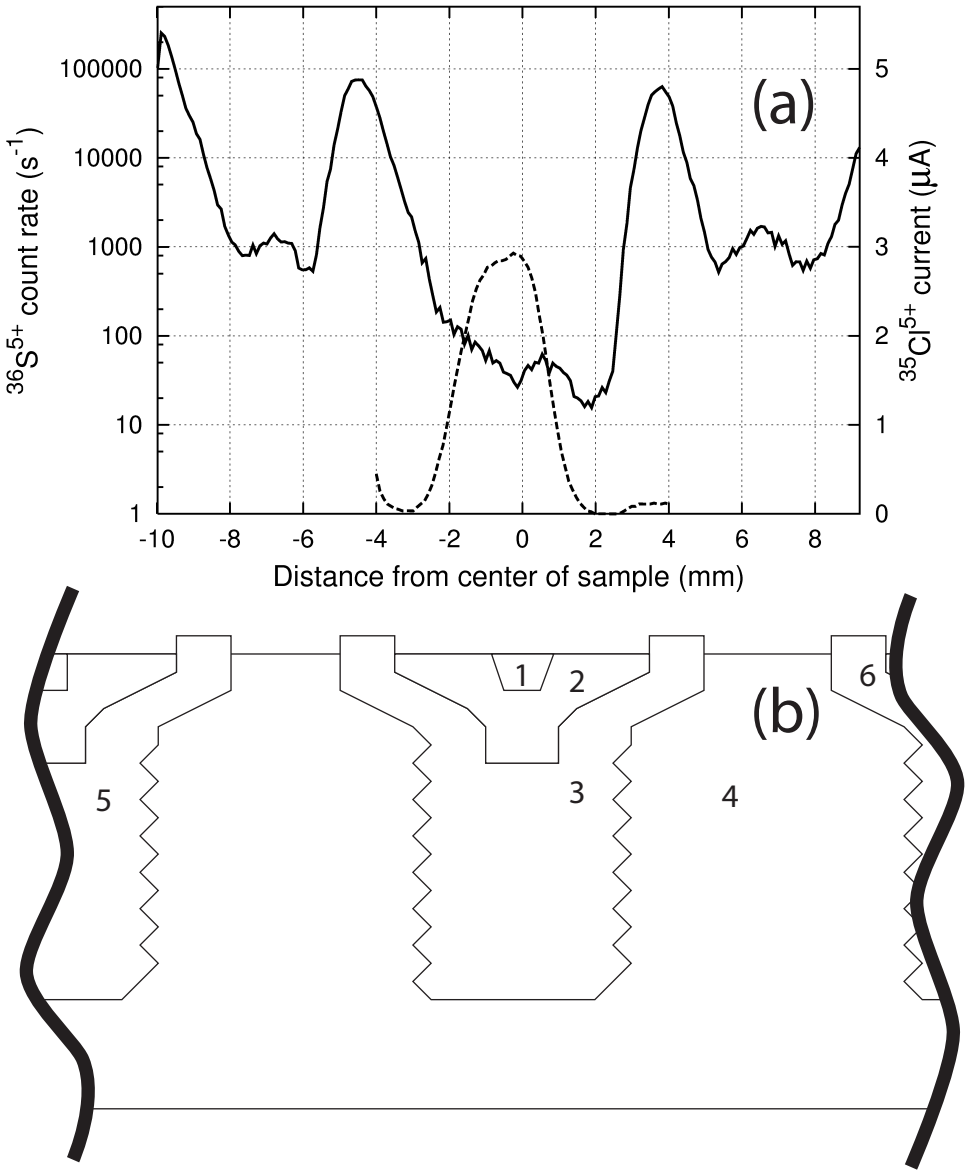
(a)
100000
10000
1000
100
10
1
5
4
3
2
1
0
-10
-8
-6
-4
-2
0
2
4
6
8
$^{36}S^{5+}$ count rate ($s^{-1}$)
$^{35}Cl^{5+}$ current (μA)
Distance from center of sample (mm)
(b)
1
2
3
4
5
6

Figure 5

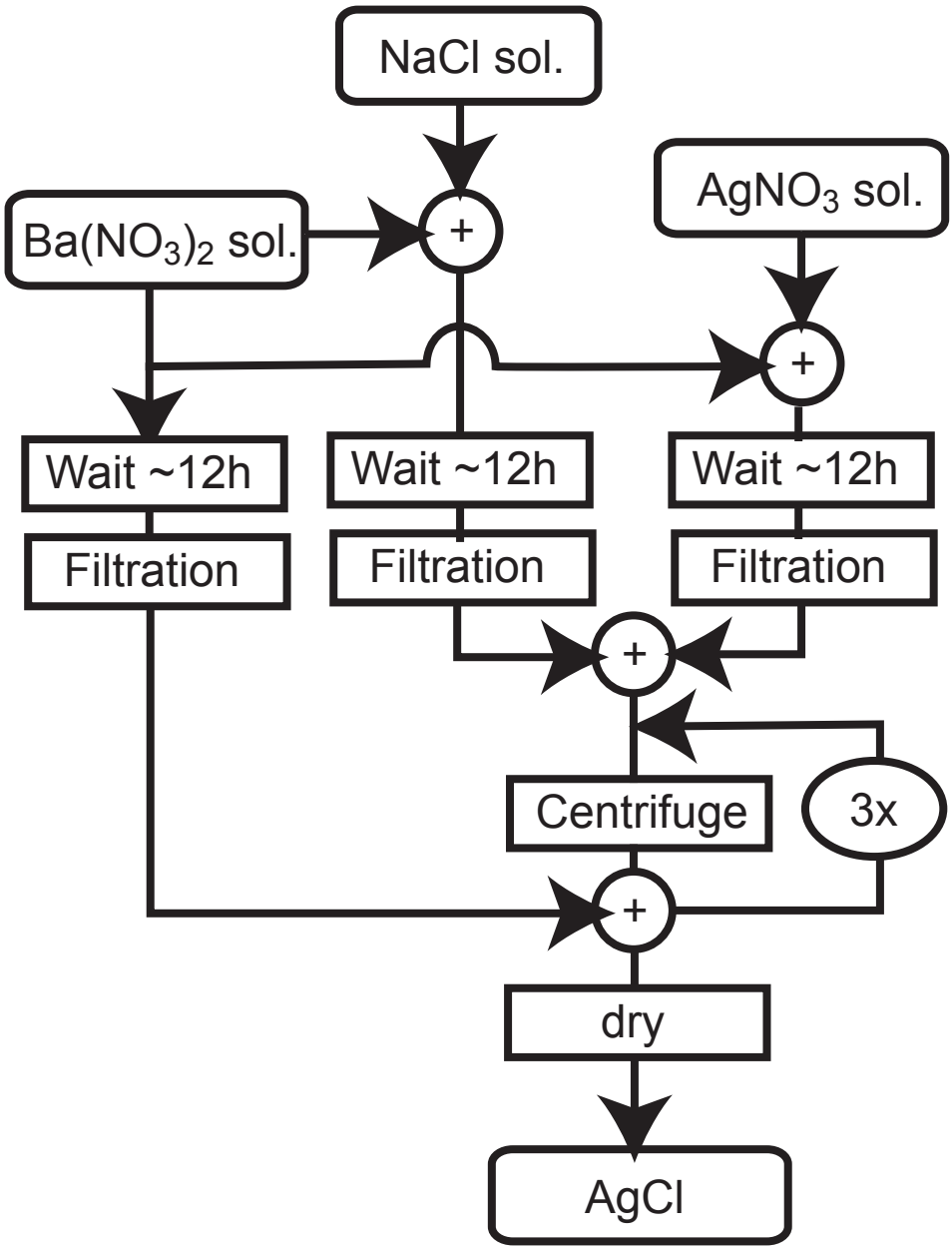
NaCl sol.
Ba(NO3)2 sol.
AgNO3 sol.
+
+
Wait ~12h
Wait ~12h
Wait ~12h
Filtration
Filtration
Filtration
+
Centrifuge
3x
+
dry
AgCl

Figure 6

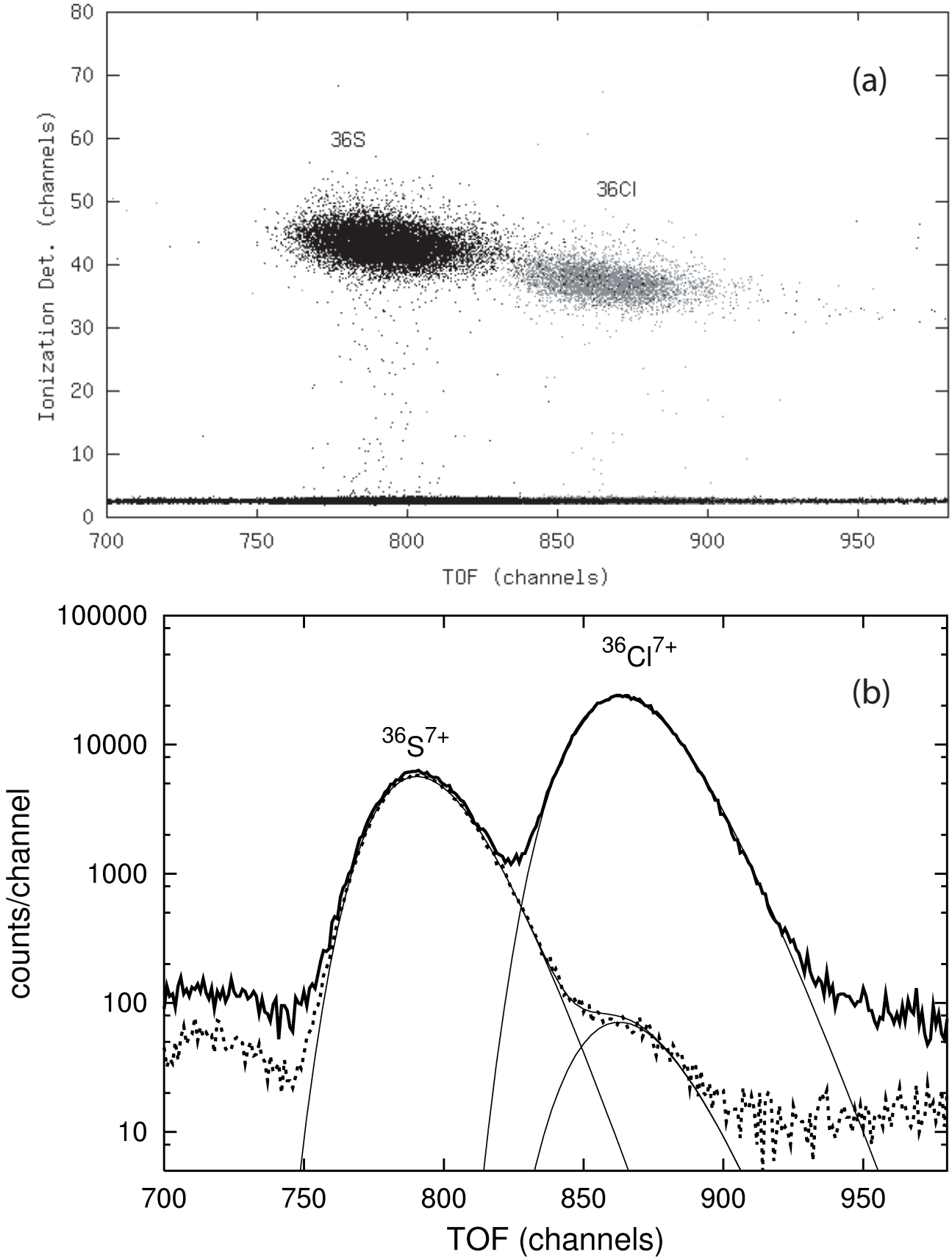
(a)
36S
36Cl
Ionization Det. (channels)
TOF (channels)
(b)
$^{36}Cl^{7+}$
$^{36}S^{7+}$
counts/channel
TOF (channels)

Figure 7